International Journal of Microwave and Wireless Technologies

cambridge.org/mrf

Rotman lens design and optimization for 5G applications

S. E. Ershadi[1], A. Keshtkar[1], A. Bayat[1], A. H. Abdelrahman[2] and H. Xin[3]

[1]Electrical Engineering Department, Faculty of Engineering and Technology, Imam Khomeini International University, Qazvin 34148-96818, Iran; [2]Department of Electrical, Computer, and Energy Engineering, University of Colorado Boulder, Boulder, CO 80309-0425, USA and [3]Department of Electrical and Computer Engineering, University of Arizona, Tucson, AZ 85721-0104, USA

Research Paper

Cite this article: Ershadi SE, Keshtkar A, Bayat A, Abdelrahman AH, Xin H (2018). Rotman lens design and optimization for 5G applications. *International Journal of Microwave and Wireless Technologies* **10**, 1048–1057. https://doi.org/10.1017/S1759078718000934

Received: 9 October 2017
Revised: 21 May 2018
Accepted: 24 May 2018
First published online: 26 June 2018

Key words:
5G; antenna design; microwave measurements; modeling and measurements

Author for correspondence:
S. E. Ershadi, E-mail: S906190001@edu.ikiu.ac.ir

Abstract

The next generation of wireless networks (5G) employs directional transmission at millimeter wave (mmW) frequencies to provide higher bandwidth and faster data rates. This is achieved by applying antenna arrays with proper beam steering capabilities. Rotman lens has long been used as a lens-based beamformer in electronically scanned arrays and its efficient design is important in the overall performance of the array. Minimizing the phase error on the aperture of the antenna array is an important design criterion in the lens. In this paper, a 7×8 wideband Rotman lens is designed. Particle swarm optimization is applied to minimize the path length error and thereby the phase error. The optimized lens operates from 25 to 31 GHz, which covers the frequency bands proposed by the Federal Communications Commission for 5G communications. The proposed optimized lens shows a maximum phase error of <0.1°. The proposed Rotman lens is a good candidate to be integrated with wideband microstrip patch antenna arrays that are suitable for 5G mmW applications.

Introduction

Due to the increasing demand for higher data rates and bandwidth, the next generation of mobile communications (5G) is migrating to millimeter wave (mmW) frequencies. To overcome the innate high path loss and atmospheric absorption at these frequency bands, highly directional transmission is necessary. Therefore, adaptive antenna arrays with efficient beamforming network (BFN), as well as good beam steering capabilities, are employed to combine signals of antenna array elements into a pattern, which is more directive than the single element pattern. A BFN usually consists of a set of input and output ports arranged along an arc. Each input port at the focal surface produces a desirable amplitude and phase distribution so that the beam is directed into a specific angle.

The concept of microwave lens was introduced in 1950 [1]. This concept was later used by Rotman and Turner to introduce the first three-focal-point lens-based BFN, known as Rotman lens, to feed linear arrays [2]. It is composed of a parallel conducting plate fed by horn antennas along the beam contour. Transmission lines were used to connect the inner receiver contour and the outer phased arrays. The three focal points on the beam contour generate zero theoretical phase errors along the phase front of the array. In the initial design, air-filled parallel plate, the beam contour was circular and the array scan angle was equal to the subtended beam port angle. Due to simplicity, reliability, and wide-scanning angle over a broad frequency bandwidth [3], the original Rotman lens design has been the bench mark for many later studies and modifications, such as size reduction [4], scan angle increment [5–7], side wall absorption reduction [8, 9], maximizing the coupling power from the feed contour to the array contour [10], and phase performance improvement [11].

One important design parameter, which could degrade the system performance in case of inefficient design, is the phase error that implies on the aperture of the array antenna [12]. Accordingly, the lens design should be optimized for the minimum possible phase error. Some research efforts have been reported on phase error reduction and optimization. In [13] phase errors reduction was performed by introducing the ratio of the scan and beam subtended angles (γ), which provided a new degree of freedom compared with the conventional design. In [14], path length errors for two-dimensional scanning were reduced by replacing the planar feed locus with a curved feed locus. In conventional Rotman lens [2], the beam and array contours are assumed to be circular. In [15], Hansen reduced the phase errors by introducing an elliptical beam contour. For each beam direction in [16, 17], feed curve points were obtained assuming zero path length error at three chosen points of the radiating array. In [3], a non-focal design scheme was applied to produce minimum average phase errors for all beam ports, rather than achieving zero-phase error for only selected

CAMBRIDGE UNIVERSITY PRESS

Table 1. Comparison of path length error reduction and design methodology of some Rotman lenses in literature

Ref.	Design methodology	Maximum path length error normalized to focal length (f_0)
[13]	Introducing ray to beam angle ratio	1.5×10^{-3}
[14]	Introducing curved feed locus	6.5×10^{-4}
[2]	Applying circular beam and array contours	2.5×10^{-3}
[15]	Introducing eccentricity	NA
[16, 17]	Obtaining feed curve points assuming zero path length error at three points of the radiating array for each beam direction	1×10^{-3}
[3]	Introducing non-focal design	NA
[18]	Introducing symmetry non-focal lens	NA
[19]	Optimizing α, F, and γ and moving off-axis focal points along the beam curve	6.5×10^{-3}
[20,21]	Optimizing transmission line lengths in three-focal scenario and updating the location of the input and output ports	1.72×10^{-5}
[22]	Determine the beam's location by applying ray optics theory	1.67×10^{-3}
[23]	Optimizing the position of the input and output ports of the lens based on genetic algorithm	3.7×10^{-5}
This paper	Optimizing the parallel plate for minimum phase error, based on PSO algorithm, over four geometrical parameters.	2.68×10^{-6}

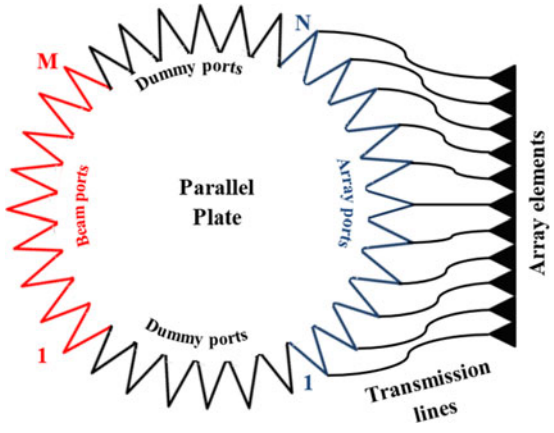

Fig. 1. Structure of a microstrip Rotman lens.

focal points. In [18], the symmetry of non-focal lens is introduced, so that the input ports and output ports can be interchangeable. In [19], the phase errors are minimized by finding the optimal values of off-center focal angle (α), On-axis focal length (f) and ray to beam angle ratio (γ) and moving off-axis

Table 2. Geometrical parameters of a trifocal Rotman lens

Parameter	Definition	Parameter	Definition
C_B	Beam contour	ψ_α	Array scan angle corresponding to α
C_A	Array contour	γ	Ray to beam angle ratio, $Sin\psi_\alpha/Sin\alpha$
F_1, F_2	Off-axis focal points	Θ	Beam port subtended angle
F	Off-axis focal length	ψ_Θ	Array scan angle corresponding to Θ
F_0	On-axis focal point	L_0	Transmission line length between point "O" and radiating element
f_0	On-axis focal length	L	Transmission line length between point "P" and radiating element
P	A desired point on the beam contour, $P(x_B, y_B)$	L_N	Normalized relative transmission line length, $(L - L_0)/f_0$
Q	A desired point on the array contour, $Q(x_A, y_A)$	D	Array aperture
H	PO length	Y	Distance from the axis of the lens
B	Focal ratio, f/f_0	F_D	Focal to aperture length ratio, f_0/D
ε_r	Dielectric constant of cavity region	A	Semi-minor axis of the beam contour ellipse
ε_e	Dielectric constant of the delay lines region	B	Semi-major axis of the beam contour ellipse
ε_i	Dielectric constant of the radiating array region	e	Eccentricity, $\sqrt{1-(A^2/B^2)}$
A	Off-center focal angle	d	Element Spacing

focal points along a beam curve. In [20, 21], a three-focal lens was converted to a non-focal lens by optimizing the length of the transmission lines in three-focal scenario, using particle swarm optimization, and updating the location of input and output ports. The method, demonstrated in [22], did reduce the phase error based on ray optics theory for determining the beam's location. In [23], genetic algorithm is used to optimize the position of the lens input and output ports for minimum phase error. Table 1 summarizes the results of these published efforts.

In this paper, we introduce a novel design of a Rotman lens for 5G applications, in terms of reducing the phase error at the output ports over a wideband operational frequency. The proposed lens covers the frequency bands considered by the Federal Communications Commission (FCC) for next-generation

https://doi.org/10.1017/S1759078718000934 Published online by Cambridge University Press

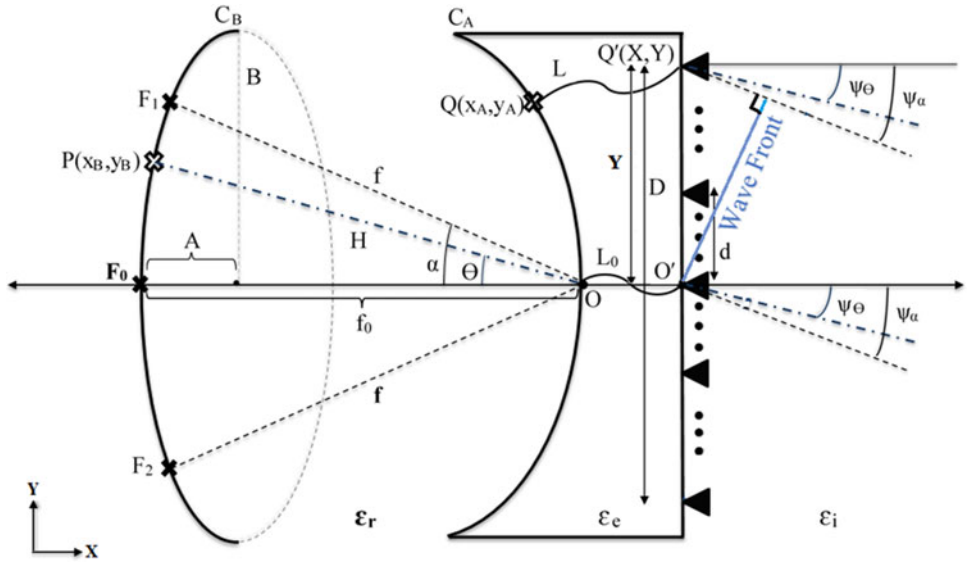

Fig. 2. The schematic geometry of a trifocal Rotman lens.

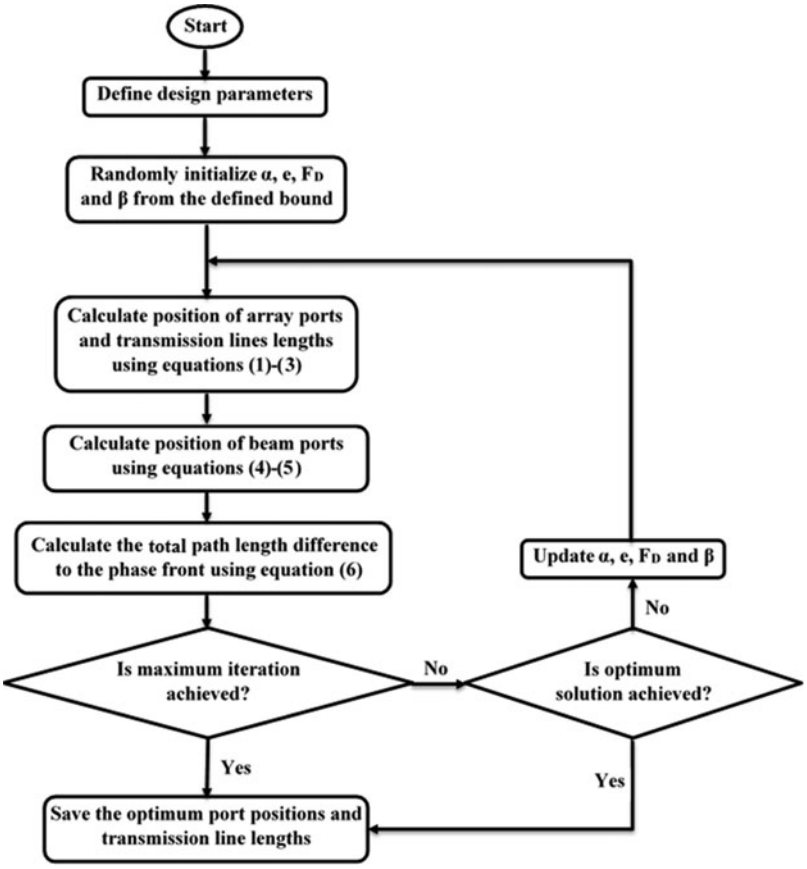

Fig. 3. The proposed optimization procedure.

Mobile Radio Services, i.e. 24.25–24.45 GHz, 25.05–25.25 GHz, and the Local Multipoint Distribution Service (LMDS) frequency bands operating at frequencies 27.5–28.35 GHz, 29.1–29.25 GHz, and 31–31.3 GHz [24]. A new design scheme is applied to minimize the phase errors on the aperture of the array antenna. By employing particle swarm optimization, the optimal values of some design parameters (i.e., eccentricity, focal to aperture length ratio, focal ratio, and off-center focal angle) are obtained, so that the corresponding input and output ports provide the minimum path length errors on the aperture of the array antenna. Because the optical path length equality and the lens geometry are used to calculate the optimization cost function, the input and output ports are indirectly involved in the optimization process.

https://doi.org/10.1017/S1759078718000934 Published online by Cambridge University Press

Table 3. Specification of the desired 5G Rotman lens

Parameter	Description	Value
f_c	Design frequency	28 GHz
ψ_α	Maximum scan angle	30°
M	Number of beam ports	7
N	Number of array ports	8
ϵ_r	Dielectric constant	2.2
tan σ	Loss tangent	0.0009
$d_{element}$	Element spacing	$\lambda_c/2$
T	Dielectric thickness	0.787 mm

Table 4. Parameters of the PSO algorithm

Parameter	Value
No. of particles	50
Particle lower bound [e, F_D, β, α]	[0, 0.5, 0.8, 19]
Particle upper bound [e, F_D, β, α]	[0.99, 3, 1.2, 30]
No. of iterations	1000
Personal adjustment weight (C_1)	1.49
Social adjustment weight (C_2)	1.49

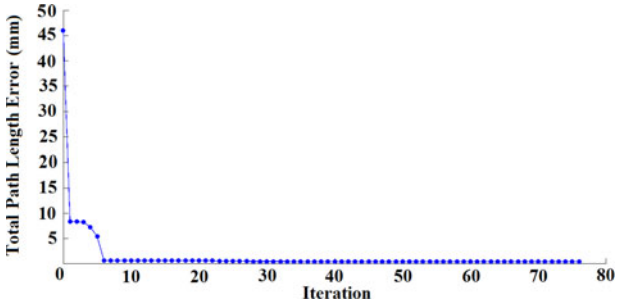

Fig. 4. The iterative optimization process.

Rotman lens structure

The structure of a microstrip Rotman lens is shown in Fig. 1. It usually consists of M number of input ports and N number of output ports to feed N number of array elements [25]. The signal applied to each input port is transmitted and picked up by all the output ports. A linear progressive phase shift is generated across the output ports of the lens due to the electrical length difference between each input port and all output ports. Rotman lens is considered as a true-time delay device as the desired phase front at the array input is provided by applying path delay mechanism within the lens cavity [26]. The path-length design mechanism in the lens is independent of frequency [25]. This characteristic makes it ideal for many broadband applications which require wide-angle scanning over a broad frequency bandwidth [27, 28]. To reduce the standing waves and multiple reflections, absorptive ports (dummy ports) are applied as shown in Fig. 1.

Table 5. Optimized parameters

Parameter	Optimized value
E	0.0031
F_D	2.976
B	0.908
α (degree)	25.01

The schematic geometry of a trifocal Rotman lens is shown in Fig. 2 and its defining geometrical parameters are presented in Table 2. The input and output ports are located on C_B and C_A, respectively. On-axis focal point F_0 and off-axis focal points F_1 and F_2 are located on the beam contour at angles of 0, +α, and −α respectively, i.e. the coordinates of $(-f_0, 0)$, $(-f\cos\alpha, f\sin\alpha)$, and $(-f\cos\alpha, -f\sin\alpha)$ [2].

Using optical path length equality [2, 3, 29], the quadric lens equation can be derived as:

$$\frac{a\varepsilon_e}{\varepsilon_r}L_N^2 + b\sqrt{\frac{\varepsilon_e}{\varepsilon_r}}L_N + c = 0$$
$$(L_N)_{1,2} = \sqrt{\frac{\varepsilon_r}{\varepsilon_e}}\frac{-b \pm \sqrt{b^2-4ac}}{2a}, \quad (1)$$

where

$$a = -1 + \left(\frac{1-\beta}{1-\beta\cos\alpha}\right)^2 + \frac{\varepsilon_i}{\varepsilon_r}\left(\frac{Y\gamma}{\beta f_0}\right)^2,$$
$$b = -2 + \frac{2\varepsilon_i}{\beta\varepsilon_r}\left(\frac{Y\gamma}{f_0}\right)^2 + \frac{2(1-\beta)}{1-\beta\cos\alpha} - \frac{\varepsilon_i}{\varepsilon_r}\left(\frac{Y\gamma\sqrt{1-\beta}\sin\alpha}{f_0(1-\beta\cos\alpha)}\right)^2,$$
$$c = \frac{\varepsilon_i}{\varepsilon_r}\left(\left(\frac{Y\gamma}{f_0}\right)^2 - \frac{(Y\sin\psi_a)^2}{f_0^2(1-\beta\cos\alpha)} + \frac{(Y\sin\psi_a)^4}{4\varepsilon_r f_0^4(1-\beta\cos\alpha)^2}\right). \quad (2)$$

The array port positions, x_A and y_A, are obtained as

$$x_A = \frac{L_N(1-\beta)}{\beta\cos\alpha - 1}\sqrt{\frac{\varepsilon_e}{\varepsilon_r}} + \frac{\varepsilon_i Y^2\sin^2\psi_a}{2\varepsilon_r f_0^2(\beta\cos\alpha - 1)},$$
$$y_A = \frac{Y\gamma}{f_0}\sqrt{\frac{\varepsilon_i}{\varepsilon_r}}\left(1 - \frac{L_N}{\beta}\sqrt{\frac{\varepsilon_e}{\varepsilon_r}}\right). \quad (3)$$

In order to have wide angle scanning capabilities, it is necessary to place some other feeds at non-focal points. This causes a phase error in the corresponding wave front [30]. Ellipse equation is used to obtain these non-focal feed points, i.e. (x_B, y_B) as:

$$x_B = \frac{A - 1 + \sqrt{A^2 + 1 - 2A + (2A-1)\left[tg^2\theta(1-e^2) - 1\right]}}{1 + (1-e^2)tg^2\theta},$$
$$y_B = -x_B(tg\theta). \quad (4)$$

https://doi.org/10.1017/S1759078718000934 Published online by Cambridge University Press

Table 6. Port positions and transmission line length

	Position (mm)			Position (mm)			
Input Port	*X*	*y*	Output port	*x*	*y*	Transmission line	Length (mm)
P_1	−102.05	−35.14	P_8	−5.29	28.34	TL_8, TL_{15}	6.92
P_2	−107.14	−24.08	P_9	−2.70	20.39	TL_9, TL_{14}	6.16
P_3	−110.29	−12.24	P_{10}	−0.97	12.29	TL_{10}, TL_{13}	5.64
P_4	−111.35	0	P_{11}	−0.11	4.11	TL_{11}, TL_{12}	5.38
P_5	−110.29	12.24	P_{12}	−0.11	−4.11		
P_6	−107.14	24.08	P_{13}	−0.97	−12.29		
P_7	−102.05	35.14	P_{14}	−2.70	−20.39		
			P_{15}	−5.29	−28.34		

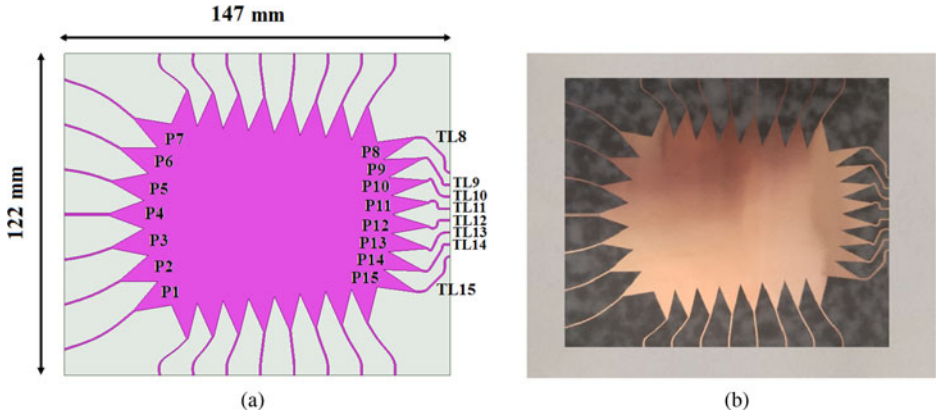

Fig. 5. Proposed 7 × 8 Rotman lens; (a) Simulation model and (b) fabricated prototype.

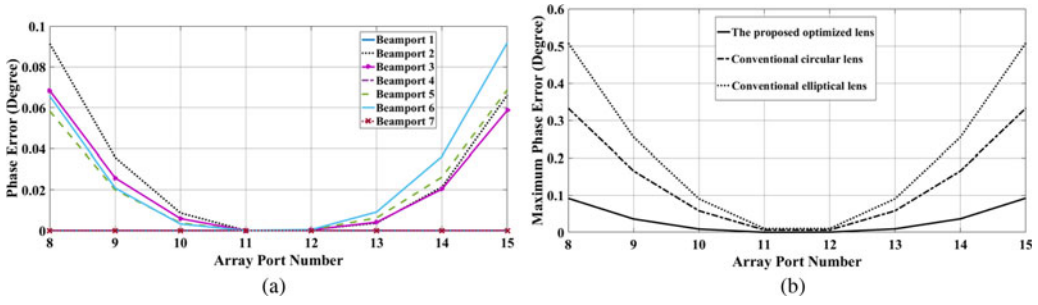

Fig. 6. (a) Phase error at the array ports (b) Comparison of the maximum phase errors of the proposed lens with conventional three-focal circular and elliptical lenses.

where A and B are the semi-minor and semi-major axes of the beam contour ellipse respectively and e is the ellipse eccentricity that measures how much the conic section deviates from being circular.

$$B = \frac{1}{2}\frac{-f_0^2\beta^2\cos^2\alpha + 2\beta f_0\cos\alpha + f_0^2\beta^2(e^2-1)\sin^2\alpha - 1}{\sqrt{1-e^2}(f_0\beta\cos\alpha - 1)},$$
$$A = B\sqrt{1-e^2} \quad (5)$$

Rotman lens design using particle swarm optimzation

Particle swarm optimization is a population-based evolutionary search algorithm that solves numerical problems by using the directional information to locally converge to the target value.

In this optimization technique, the population, known as a swarm, is composed of search points, known as particles. Each particle has a position and a velocity for each of its dimensions. The optimum is looked for by iteratively updating the swarm. In each iteration, the movement of the swarm is guided by updating the velocity of each particle according to its personal best position (*p*best), i.e. the position at which each particle achieved

https://doi.org/10.1017/S1759078718000934 Published online by Cambridge University Press

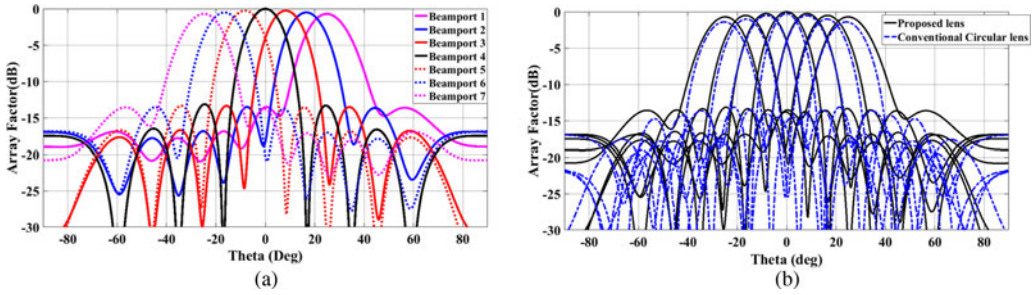

Fig. 7. Array factor (a) Proposed lens (b) Comparison with conventional circular lens.

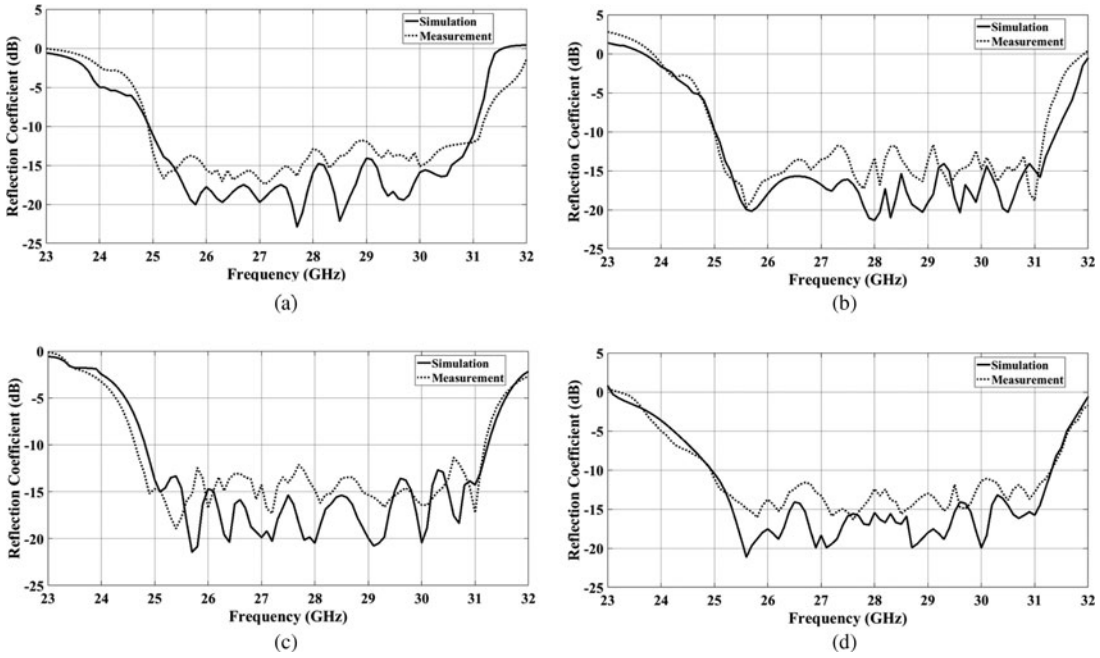

Fig. 8. Reflection coefficient of the proposed optimized lens (a) port 1, (b) port 2, (c) port 3, (d) port 4.

Table 7. Angle of the produced beam in different lenses

Input Port	Ideal beam angle	Conventional circular lens beam angle	Elliptical lens beam angle	Proposed lens beam angle
P_1	−24.9	−24.06	−23.95	−24.92
P_2	−16.6	−16.3	−16.2	−16.61
P_3	−8.3	−8.17	−8.08	−8.329
P_4	0	0.091	0.15	0.045
P_5	8.3	8.17	8.08	8.329
P_6	16.6	16.3	16.2	16.61
P_7	24.9	24.06	23.95	24.92

the best solution up to the current iteration, and the global best position of the entire swarm (*g*best), i.e. the position at which the best fitness value has been obtained so far by any particle among pbests [31]. This iterative process is repeated until a termination criterion is met, i.e. the maximum defined number of iterations is performed or an optimum solution is eventually achieved. Particle swarm optimization (PSO) has some advantages compared with other optimization techniques (e.g., genetic algorithm (GA) technique), which are mainly in its algorithmic simplicity and its ability to control convergence [32]. PSO is based upon the behavior of social swarm, which requires only one operator, i.e., velocity. On the other side, GA is based on genetic coding and natural selection, which requires three operators of selection, crossover, and mutation [32].

We used PSO algorithm, implemented on MATLAB, to avoid time-consuming in using the commercial software optimization process. In the study under consideration, the search space consists of four-dimensional particles, i.e. each particle is an array of four parameters. These four parameters, namely e, F_D, β, and α are considered optimization parameters since they have a direct effect on the shape of the beam and array contours, port positions, and the phase performance of the lens [2].

Total path length difference to the phase front is considered for minimization to evaluate the achieved parameters in each iteration. For each port position on the beam contour, $P(x_B, y_B)$, a path length error can be obtained by the difference in path length from P through Q and Q' to the phase front, and from P through

https://doi.org/10.1017/S1759078718000934 Published online by Cambridge University Press

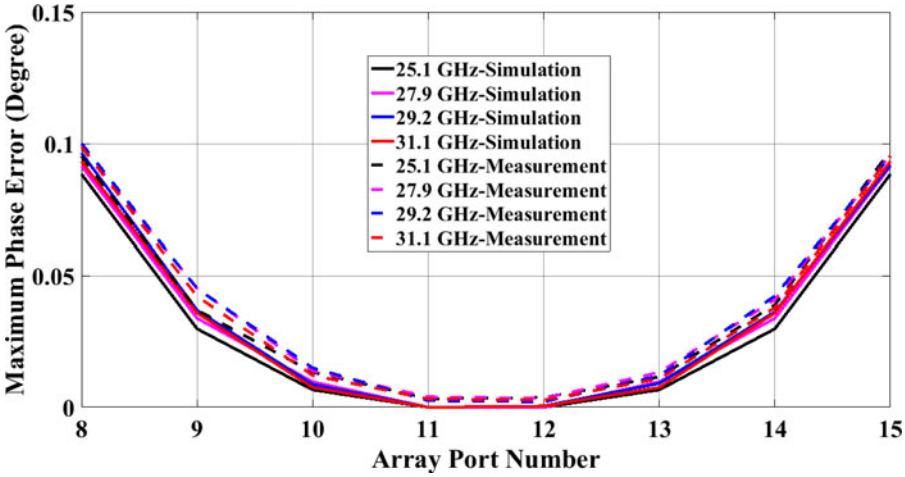

Fig. 9. Maximum phase error at the output ports, for the center frequencies recommended by FCC.

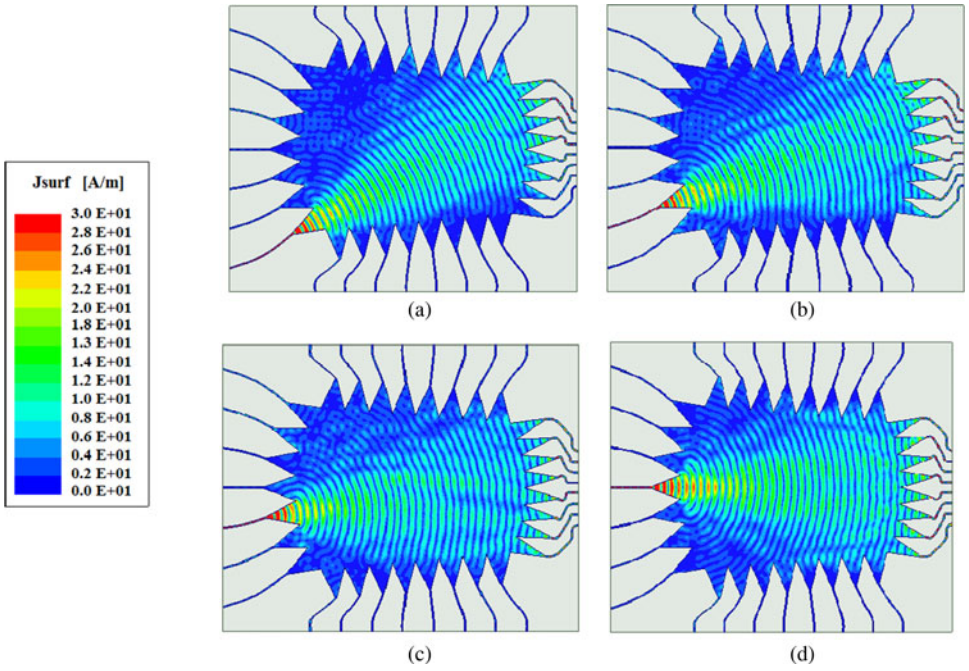

Fig. 10. Current distribution of the proposed optimized Rotman lens with (a) Port 1, (b) Port 2, (c) Port 3, (d) port 4 excited.

O and O' to the phase front:

$$\Delta l = PQ\sqrt{\varepsilon_r} + L\sqrt{\varepsilon_e} + Y\sqrt{\varepsilon_i}\sin\psi_\theta - (PO + L_0), \qquad (6)$$

where $Q(x_A, y_A)$ is any port position along the array contour and Y is the coordinate of the corresponding element on the antenna array.

Particles move through the search space and look iteratively for the optimum values of e, F_D, β, and α by which the optimum port positions and transmission line lengths are calculated, i.e. the total path length error and phase error are minimized.

Figure 3 illustrates the flowchart of the proposed procedure. After defining the design parameters and the initial values, the positions of the array ports, beam ports, and transmission lines lengths are exactly obtained from (1) to (5). In the next step, the path length errors are obtained using (6) and summed up to obtain the total path length error. The optimization parameters are then updated using PSO algorithm and substituted in (1)–(5) to update port positions and transmission lines lengths. This procedure is continued so that the minimum total path length error is achieved. In the last step, the optimum port positions and transmission line lengths that provide the minimum total path length error are saved.

Based on measurements and analysis performed by NYU Wireless for 5G communications [33–47], it is recommended that the base station antenna should achieve a high gain of 20 dBi at the broadside direction, and a look angle of 60° based on beam steering capability with steps of 8°–10° in azimuth plane. Consequently, seven steered beams of a10° step (i.e., −30°, −20°, −10°, 0°, +10°,+20°, and +30°) are needed, which are implemented by placing seven input ports in the proposed Rotman lens. Moreover, the 1×4 subarray antenna, which is designed for wideband 5G applications and is presented in [48], achieves a gain of more than 11 dBi over the entire band. Based

https://doi.org/10.1017/S1759078718000934 Published online by Cambridge University Press

on array theory [49], eight elements separated by a half-wavelength achieves an array factor of 10*log(8) = 9 dB. Accordingly, eight of this subarray antenna can achieve the required gain of 20 dBi, which is implemented by defining eight output ports in the proposed Rotman lens. The design criteria chosen to minimize the phase error in the lens and the geometrical and electrical properties of the dielectric substrate (RT Duroid 5880) are listed in Table 3.

The parameters of the PSO algorithm and their values are listed in Table 4. Path length error is considered for minimization in the optimization process. As shown in Fig. 4, the optimization process stops after 76 iterations when the value of the objective function, i.e. the total path length error, stops improving 0.4404 mm.

The optimized parameters and their values are listed in Table 5, and the position of the input and output ports, as well as the transmission line lengths, are listed in Table 6.

Simulation and measurement results

To validate the proposed optimization process, the optimized Rotman lens is first simulated using HFSS simulation software and then fabricated and measured according to the port positions and the transmission line lengths mentioned in Table 6. The simulated model and fabricated prototype are illustrated in Fig. 5.

Figure 6(a) depicts the phase error between the beam-ports and the array-ports of the proposed optimized lens. As observed, the phase error of the focal ports (i.e. ports 1, 4, and 7), are approximately zero, whereas the phase error is increased at the other ports. The aim of the proposed method is to minimize the phase error of all ports.

Figure 6(b) compares the maximum phase errors of the lens designed by the proposed method with the conventional three-focal circular and elliptical designs. As can be seen, the proposed optimization reduces the maximum phase error to <0.1°, i.e. 3–5 times better than the conventional methods. This reduction in phase error guarantees precise beam-steering capability when the lens feeds an antenna array, as shown in Fig. 7. This figure presents the array factor patterns, based on applying the phase control capability of the proposed lens on a linear array of eight elements separated by a half-wavelength at the center frequency, i.e., 28 GHz. As seen, the proposed lens can achieve a scanning range of ± 34° with steps of approximately 8.3°. A comparison of array factors of the proposed lens and conventional circular and elliptical lenses are demonstrated in Fig. 7(b) and Table 7. As seen, the produced beam angles are very close to the ideal condition, where the array factor varies up to 1.6 dB at broadside over the operational bandwidth, i.e. 25–31 GHz.

Figure 8 shows the simulated and measured reflection coefficients of ports 1–4 of the proposed lens. Due to symmetry, the reflection coefficient of ports 5–7 are equal to ports 3–1, respectively. An average impedance bandwidth of 21.4% (25–31 GHz) is achieved. The obtained wide bandwidth covers most of the mmW Gbps Broadband (MGB) candidates, considered by the FCC for next-generation Mobile Radio Services, i.e. 25.05–25.25 GHz and the LMDS frequency bands operating at frequencies 27.5–28.35 GHz, 29.1–29.25 GHz, and 31–31.3 GHz. Simulation and measurement results of the maximum phase errors at the output ports are shown in Fig. 9, so that all frequency bands recommended by FCC are demonstrated. As seen, the measurement results are in good agreements with simulations, thereby validating the precise phase control capability of the proposed Rotman lens, which ensures a beam steering functionality when connected to an antenna array.

Figure 10 shows the distribution of the current propagating through the lens when ports 1–4 are excited separately. It can be observed that the wave front arrives at all the array ports as most of the electric field propagates to output ports, scattered waves are absorbed in dummy ports and coupling effect between input ports is nearly zero.

Conclusion

In this paper, the parallel plate of Rotman lens is optimized for minimum phase error by applying PSO algorithm over four geometrical parameters, i.e. eccentricity (e), focal to aperture length ratio (F_D), focal ratio (β), and off-center focal angle (α). Input and output port positions, and transmission lines lengths were then calculated by the three-focal scenario. To evaluate the proposed method, full-wave simulation of a Rotman lens with 7 input and 8 output ports was performed at 28 GHz followed by fabrication of the simulated model. The proposed optimization technique reduces the maximum phase error to <0.1°, i.e. 3–5 times reduction in the maximum phase error. The lens showed an ability to scan −34° to 34° with steps of 8.3° and with beam angles which are very close to the ideal condition in comparison with conventional lenses in literature. Moreover, the proposed design achieves a wide impedance bandwidth of approximately 21.4% (25–31 GHz), which covers most of the mmW Gbps Broadband frequency bands considered by the FCC for next-generation Mobile Radio Services. The proposed Rotman lens can be integrated with wideband microstrip patch antenna arrays which are suitable for 5G mmW applications.

References

1. **Ruze J** (1950) Wide-angle metal-plate optics. *Proceedings IRE*, **38**, 53–59.
2. **Rotman W and Turner RF** (1963) Wide-angle microwave lens for line source applications. *IEEE Transactions on Antennas Propagation* **11**, 623–632.
3. **Dong J, Zaghloul AI and Rotman R** (2010) Phase-error performance of multi-focal and non-focal two-dimensional Rotman lens designs. *IET Microwaves, Antennas and Propagation* **4**, 2097–2103.
4. **Archer DH and Maybell MJ** (2005) Rotman lens development history at Raytheon Electronic warfare systems 1967–1995. *IEEE Antennas Propag. Soc. Int. Symp., Washington D.C., USA*.
5. **Smith MS** (1982) Design considerations for Ruze and Rotman lens. *Radio and Electronic Engineer* **52**, 181–187.
6. **Smith MS** (1983) Amplitude performance of Ruze and Rotman lenses. *Radio and Electronic Engineer*, **53**, 329–336.
7. **Gagnon DR** (1989) Procedure for correct refocusing of the Rotman lens according to Snell's law. *IEEE Transactions on Antennas and Propagation* **37**, 390–392.
8. **Musa L and Smith M** (1986) Microstrip Rotman lens port design. *Antennas and Propagation Society International Symposium, Philadelphia, USA*.
9. **Musa L and Smith MS** (1989) Microstrip port design and sidewall absorption for printed Rotman lenses. *IEE Proceedings H: Microwaves Antennas Propagation* **136**, pp. 53–58.
10. **Singhal PK, Sharma PC and Gupta RD** (2003) Rotman lens with equal height of array and feed contours. *IEEE Transactions on Antennas and Propagation* **51**, 2048–2056.
11. **Dong J, Zaghloul AI and Rotman R** (2008) Non-focal minimum phase-error planar Rotman lens. *USNC/URSI National Radio Science Meeting, Colorado, USA*.

https://doi.org/10.1017/S1759078718000934 Published online by Cambridge University Press

12. **Vashist S, Dutta U and Soni MK** (2012) Design and performance analysis of Rotman lens. *International Journal of Engineering Research and Applications* **2**, 1792–1795.
13. **Katagi T, Mano S and Sato S** (1984) An improved design method of Rotman lens antennas. *IEEE Transactions on Antennas Propagation* **32**, 524–527.
14. **Rappaport C and Zaghloul A** (1985) Optimized three-dimensional lenses for wide-angle scanning. *IEEE Transactions on Antennas Propagation* **33**, 1227–1236.
15. **Hansen RC** (1991) Design trades for Rotman lenses. *IEEE Transactions on Antennas Propagation* **39**, 464–472.
16. **Uyguroglu R and Oztoprak AY** (2009) A method for minimizing the phase errors of Rotman lenses. *International Conference Electrical and Electronics Eng., Bursa, Turkey*.
17. **Uyguroglu R, Oztoprak AY and Ergun C** (2012) Improved phase performance for Rotman lens. *Int. Journal of RF and Microwave Computer-Aided Engineering* **23**, 634–638.
18. **Rajabalian M and Zakeri B** (2012) Non-focal microwave lens design with optimization of phase errors and amplitude performance. *20th Telecommunications Forum (TELFOR), Belgrade, Serbia*.
19. **Park J and Park D** (2013) Phase error minimization by refocusing Rotman lens. *Proc. of the Asia-Pacific Microwave Conference, Seoul, South Korea*.
20. **Rajabalian M and Zakeri B** (2012) An implemented non-focal Rotman lens. *Radar Conference (EuRAD), Paris, France, September 9–11*.
21. **Rajabalian M and Zakeri B** (2015) Optimisation and implementation for a non-focal Rotman lens design. *IET Microwaves Antennas Propagation* **9**, 982–987.
22. **Attaran A, Rashidzadeh R and Kouki A** (2016) 60 GHz low phase error Rotman lens combined with wideband microstrip antenna array using LTCC technology. *IEEE Transactions on Antennas Propagation*. **64**, 5172–5180.
23. **Darvazehban A, Manoochehri O, Salari M, Dehkhoda P and Tavakoli A** (2017) Ultra-wideband scanning antenna array with Rotman lens. *IEEE Transactions on Microwave Theory Techniques* **65**, 3435–3442.
24. **FCC** (2015) FCC 15-138, (2015, Oct. 23), Available at: https://apps.fcc.gov/edocs_public/attachmatch/FCC-15-138A1.pdf.
25. **Archer D** (1975) Lens-fed multiple-beam arrays. *Microwave Journal* **18**, 37–42.
26. **Jafari AH, Liu W and Morgan DR** (2013) Study of sensor positions for broadband beamforming. *IEEE Signal Processing Letters* **20**, 779–782.
27. **Hawesand M and Liu W** (2014) Sparse array design for wideband beamforming with reduced complexity in tapped delay-lines. *IEEE Transactions on Audio, Speech* **22**, 1236–1237.
28. **Archer DH** (1984) Lens-fed multiple beam arrays. *Microwave Journal* **27**, 171–195.
29. **Pozar DM** (1985) *Antenna Design Using Personal Computers*. USA: Artech House.
30. **Hansan RC** (1992) Array pattern control synthesis. *Proceedings of IEEE* **80**, 141–151.
31. **Zhang Y, Wang S and Jil G** (2015) A comprehensive survey on particle swarm optimization algorithm and its applications. *Mathematical Problems in Engineering*, **2015**, 1–38.
32. **Rahmat-Samii Y** (2003) Genetic algorithm (GA) and particle swarm optimization (PSO) in engineering electromagnetics. *17th International Conference Applied Electromagnetics and Communications, Dubrovnik, Croatia*.
33. **Rappaport TS, Sun S, Mayzus R, Zhao H, Azar Y, Wang K, Wong GN, Schulz JK, Samimi MK and Gutierrez F** (2013) Millimeter wave mobile communications for 5G cellular: It will work!. *IEEE Access*, **1**, 335–349.
34. **Samimi MK, Wang K, Azar Y, Wong GN, Mayzus R, Zhao H, Schulz JK, Sun S, Gutierrez F and Rappaport TS** (2013) 28 GHz angle of arrival and angle of departure analysis for outdoor cellular communications using steerable beam antennas in New York City. *IEEE 77th Vehicular Technology Conference (VTC Spring), Dresden, Germany*.
35. **Azar Y, Wong G, Wang K, Mayzus R, Schulz JK, Zhao H, Gutierrez F, Hwang D and Rappaport TS** (2013) 28 GHz propagation measurements for outdoor cellular communications using steerable beam antennas in New York City. *IEEE International Conference on Communications (ICC), Budapest, Hungary*.
36. **Sun S and Rappaport TS** (2013) Multi-beam antenna combining for 28 GHz cellular link improvement in urban environments. *IEEE Global Communications Conference (GLOBECOM), Atlanta, USA*.
37. **Maccartney GR, Zhang J, Nie S and Rappaport TS** (2013) Path loss models for 5G millimeter wave propagation channels in urban microcells. *IEEE Global Communications Conference (GLOBECOM), Atlanta, USA*.
38. **Nie S, Maccartney GR, Sun S and Rappaport TS** (2014) 28 GHz and 73 GHz signal outage study for millimeter wave cellular and backhaul communications. *IEEE International Conference on Communications (ICC), Sydney, Australia*.
39. **Sun S, Maccartney GR, Samimi MK, Nie S and Rappaport TS** (2014) Millimeter wave multi-beam antenna combining for 5G cellular link improvement in New York City. *IEEE International Conference on Communications (ICC), Sydney, Australia*.
40. **Maccartney GR, Samimi MK and Rappaport TS** (2014) Omnidirectional path loss models in New York City at 28 GHz and 73 GHz. *2014 IEEE 25th Annual International Symposium on Personal, Indoor, and Mobile Radio Communication (PIMRC), Washington D.C., USA*.
41. **Sulyman AI, Nassar AT, Samimi MK, Maccartney GR, Rappaport TS and Alsanie A** (2014) Radio propagation path loss models for 5G cellular networks in the 28 GHz and 38 GHz millimeter-wave bands. *IEEE Communications Magazine* **52**, 78–86.
42. **Maccartney GR, Rappaport TS, Samimi MK and Sun S** (2015) Millimeter-wave omnidirectional path loss data for small cell 5G channel modeling. *IEEE Access* **3**, 1573–1580.
43. **Maccartney GR, Rappaport TS, Sun S and Deng S** (2015) Indoor office wideband millimeter-wave propagation measurements and channel models at 28 and 73 GHz for ultra-dense 5G wireless networks. *IEEE Access* **3**, 2388–2424.
44. **Sun S, Thomas TA, Rappaport TS, Nguyen H, Kovacs IZ and Rodrigue I** (2015) Path loss, shadow fading, and line-of-sight probability models for 5G urban macro-cellular scenarios. *IEEE Globecom Workshops (GC Wkshps), San Diego, USA*.
45. **Sun S, MacCartney GR, Samimi MK and Rappaport TS** (2015) Synthesizing omnidirectional antenna patterns, received power and path loss from directional antennas for 5G millimeter-wave communications. *IEEE Global Communications Conference (GLOBECOM), San Diego, USA*.
46. **Sun S, MacCartney GR and Rappaport TS** (2016) Millimeter-wave distance-dependent large-scale propagation measurements and path loss models for outdoor and indoor 5G systems. *10th European Conference on Antennas and Propagation (EuCAP), Davos, Switzerland*.
47. **Samimi MK, MacCartney GR, Sun S and Rappaport TS** (2016) 28 GHz millimeter-wave ultrawideband small-scale fading models in wireless channels. *IEEE 83rd, Nanjing, China*.
48. **Ershadi S, Keshtkar A, Abdelrahman AH and Xin H** (2017) Wideband high gain antenna subarray for 5G applications. *Progress in Electromagnetics Research C* **78**, 33–46.
49. **Balanis CA** (2005) *Antenna Theory Analysis and Design*, 3rd Edn. USA: John Wiley & Sons Inc.

Seyyedehelnaz Ershadi received her B.S. and M.S. degrees from Islamic Azad University, Tehran, Iran, in 2006 and 2009, respectively. In 2014 she was awarded a scholarship by the Ministry of Science, Research and Technology of the Islamic Republic of Iran to carry out her Ph.D. research work as a research scholar at the Microwave and Millimeter Wave Laboratory, University of Arizona. She is currently studying for a Ph.D. degree in communication engineering from Imam Khomeini International University. Her main research interests include antennas, antenna arrays, millimeter wave, and 5G and broadband communications.

https://doi.org/10.1017/S1759078718000934 Published online by Cambridge University Press

Asghar Keshtkar was born in Ardabil, Iran, in 1962. He received the B.Sc. degree in electrical engineering from Tehran University, Tehran, Iran, the M.Sc. degree in electrical engineering from the University of Khaje-Nasir, Tehran, and the Ph.D. degree in electrical engineering from the Iran University of Science and Technology, Tehran, in 1989, 1992, and 1999, respectively. He is currently a Professor with the Faculty of Engineering and Technology, Imam Khomeini International University (IKIU), Ghazvin, Iran. His current research interests include electromagnetics, bioelectromagnetics, and electromagnetic launchers and antennas.

Alireza Bayat received B.E. degree in communication engineering from Andhra University, Visakhapatnam, India, in 1987; the M.Tech. and the Ph.D. degree in electrical and communication engineering from the University of IIT Banaras Hindu, Varanasi, India, in 1989, 1992, respectively. He is currently an Assistant Professor with the Faculty of Engineering and Technology, Imam Khomeini International University, Qazvin, Iran. His research interests include electromagnetic, radar, bio-electromagnetic, antenna, and EMC.

Ahmed H. Abdelrahman received B.S. and M.S. degrees from The Department of Electrical Engineering, Electronics and Communications, Ain Shams University, Cairo, Egypt, in 2001 and 2010, respectively, and he received a Ph.D. degree in engineering sciences from The Department of Electrical Engineering, University of Mississippi, University, MS, USA, in 2014. Dr. Abdelrahman is currently a research associate with the Antenna Research Group (ARG), in The Department of Electrical, Computer, and Energy Engineering, at The University of Colorado Boulder, Boulder, CO, USA. His research interests include transmitarray/reflectarray antennas, mobile antennas, reconfigurable antennas, simultaneous transmit and receive (STAR) antennas, satellite communications, and thermoacoustic and millimeter-wave imaging. Dr. Abdelrahman was the recipient of the several prestigious awards, including the Third-Place Winner Student Paper Competition Award at the 2013 ACES Annual Conference, and the Honorable Mention Student Paper Competition at the 2014 IEEE AP-S International Symposium on Antennas and Propagation.

Hao Xin received the Ph.D. degree in physics from the Massachusetts Institute of Technology (MIT), Cambridge, MA, USA, in 2001. He performed research studies for 5 years in MIT's Physics Department and at Lincoln Laboratory, where he investigated power dependence of the surface impedance of high-Tc superconducting films and Josephson junction properties at microwave frequencies. From November 2000 to November 2003, he was a Research Scientist with the Rockwell Scientific Company, Thousand Oaks, CA, USA, where he conducted research as Principal Manager/Principal Investigator in the area of electromagnetic band-gap surfaces, quasi-optical amplifiers, electronically scanned antenna arrays, and MMIC designs using various III–V semiconductor compound devices, and random power harvesting. From 2003 to 2005, he was a Sr. Principal Multidisciplinary Engineer at Raytheon Missile Systems, Tucson, AZ, USA. He is now a Professor and Director of the Cognitive Sensing Center in the Electrical and Computer Engineering Department and Physics Department at the University of Arizona, Tucson, AZ, USA. He has published more than 270 refereed technical papers in the areas of solid-state physics, photonic crystals, and the applications thereof in microwave and millimeter wave technologies. He has 13 patents issued and one pending in the areas of photonic crystal technologies, random power harvesting based on magnetic nano-particles, and microwave nano-devices. His current research focus is in the area of microwave, millimeter wave and THz technologies, including solid-state devices and circuits, antennas, passive circuits, 3-D-printed EM components and systems, and applications of new materials, such as metamaterials and carbon nanotubes.

https://doi.org/10.1017/S1759078718000934 Published online by Cambridge University Press